Multiphasic calcium signatures in the cytosol and nucleus of *Lotus japonicus* roots unlock the early discrimination of fungal signals

Filippo Binci[1], Jürgen Kleine-Vehn[2,3], Marco Giovannetti[1#], Lorella Navazio[1#]

[1]Department of Biology, University of Padova, 35131 Padova, Italy

[2]Centre for Integrative Biological Signalling Studies (CIBSS), University of Freiburg, 79104 Freiburg, Germany

[3]Institute of Biology II, Department of Molecular Plant Physiology (MoPP), University of Freiburg, 79104 Freiburg, Germany

[#]authors for correspondence. Email: marco.giovannetti@unipd.it; lorella.navazio@unipd.it

Summary

Changes in intracellular calcium concentration are known to mediate plant responses to both beneficial and detrimental microorganisms. Increasing evidence suggests that boundaries between early signalling events in plant pathogenesis and symbiosis are less defined than previously thought, given the occurrence of Ca^{2+} signals partially sharing subcellular location and dynamics.

In this study we used differentially targeted aequorin-based Ca^{2+} reporters to measure cytosolic and nuclear Ca^{2+} signatures triggered in *Lotus japonicus* roots by putative symbiotic and pathogenic fungal molecules.

By using mutants impaired in the Common Symbiotic Signalling Pathway, we dissected the multiphasic nature of the stimulus-specific Ca^{2+} transients, highlighting significant differences in the genetic components underlying the cytosolic and nuclear Ca^{2+} response to short-chain (CO4), long-chain (CO8) and lipidated (mycLCO) chitin oligomers. Moreover, a pharmacological approach shed light on the origin, modulation and interdependence of the observed Ca^{2+} fluxes.

Our analysis of the overall plant root response in terms of cytosolic and nuclear Ca^{2+} changes helps disentangling the complex communication circuits in the pre-contact signal exchange phase and enhances our quantitative understanding of how plants can perceive and discriminate different fungal molecules.

Keywords: aequorin, arbuscular mycorrhizal symbiosis, calcium, chitin oligomers, cytosol, fungal signals, *Lotus japonicus*, nucleus.

Introduction

Plant roots encounter myriads of soil microorganisms and activate distinct transcriptional and developmental programs upon the recognition of highly conserved microbial components - such as chitin or flagellin - or specific diffusible chitin-based molecules - such as Myc factors and Nod factors - driving the process towards an immunity-like response or a symbiotic program, respectively. Whereas the recognition of microbial components by the plant host relies on a network of plasma membrane receptors (Zipfel & Oldroyd, 2017), a pivotal common mediator of downstream signals is calcium. Indeed, both in the case of plant responses to pathogenic (Ranf *et al.*, 2011; Wan *et al.*, 2012; Nars *et al.*, 2013; Keinath *et al.*, 2015; Feng *et al.*, 2019; Zhang *et al.*, 2021) or to symbiotic (Navazio *et al.*, 2007; Capoen *et al.*, 2011; Genre *et al.*, 2013; Feng *et al.*, 2019; Zhang *et al.*, 2021) molecules, the intracellular calcium concentration ([Ca^{2+}]) increases with specific signatures, thereby activating a tailored downstream program. However, it is evident that crosstalks and overlaps between Ca^{2+}-mediated plant symbiotic and pathogenic intracellular responses exist and our understanding is hampered by several degrees of confounding factors at the level of signalling molecules, plant plasma membrane receptors and Ca^{2+} responses.

In the case of arbuscular mycorrhizal (AM) symbiosis, plants can detect symbiotic partners through the perception of short-chain chitin oligomers (COs), in particular tetrameric (CO4) and pentameric (CO5) chitooligosaccharides, and a mixture of lipochitooligosaccharides (LCOs) with structural similarities to rhizobial Nod factors (Maillet *et al.*, 2011; Genre *et al.*, 2013; Feng *et al.*, 2019). By contrast, plants can perceive fungal pathogens via chitin, a crucial component of the fungal cell wall, acting as pathogen-associated molecular pattern (PAMP). If a clear-cut difference between CO4/CO5 and chitin exists (Genre *et al.*, 2013), chitin oligomers with a longer chain, such as CO8, show both pathogenic and symbiotic characteristics. In fact, different experimental setups led to apparently opposite conclusions regarding the nature of those molecules (Genre *et al.*, 2013; Feng *et al.*, 2019; Zhang *et al.*, 2021). Another element adding complexity to the system is the ambiguous role of some plasma membrane receptors, such as OsCERK1, mediating plant responses to chitin, the recognition of symbiotic molecules, and the establishment and functioning of mycorrhizal roots (Miyata *et al.*, 2014; Zhang *et al.*, 2015, 2021; Carotenuto *et al.*, 2017). Altogether both the nature of fungal signals and the overlapping roles of plant plasma membrane receptors act in an intricate continuum between pathogenesis and symbiosis.

The multifaceted intracellular Ca^{2+} homeostatic machinery that relies on the contribution of different intracellular Ca^{2+} storage compartments (Stael *et al.*, 2012; Costa *et al.*, 2018; Pirayesh *et al.*, 2021) adds a further layer of complexity in the analysis of Ca^{2+} responses. The PAMP-induced cytosolic Ca^{2+} elevation is commonly considered to stem from an influx of the ion from the extracellular space and is responsible for the cellular ROS burst (Thor & Peiter, 2014; Zipfel & Oldroyd, 2017). Evidence from the early 2000s suggested that also the cytosolic Ca^{2+} elevation evoked by AM fungal and rhizobial symbiotic signals has an extracellular origin (Miwa *et al.*, 2006; Navazio *et al.*, 2007), even though this aspect has not been further investigated. On the other hand, a complex repertoire of cation channels (MtDMI1/LjCASTOR, LjPOLLUX, CNGC15) and ECA-type Ca^{2+}-ATPase (MCA8), located in the nuclear envelope, are known to be involved in the genesis of the symbiotic nuclear and perinuclear Ca^{2+} spiking (Charpentier, 2018). This process is dependent on the activation of the Common Symbiotic Signalling Pathway (CSSP) by fungal molecules (Oldroyd, 2013; Choi *et al.*, 2018; Radhakrishnan *et al.*, 2020). Therefore, it remains to be understood whether the cytosolic Ca^{2+} elevation is shared or not among those two opposite processes triggered by symbiosis and immunity signals.

In this work, we analyzed the effects induced by a set of chitin-related oligomers on cytosolic and nuclear Ca^{2+} levels in different genetic backgrounds of *Lotus japonicus* roots by using specifically targeted aequorin-based Ca^{2+} reporters. We accurately quantified the root Ca^{2+} signatures upon treatment with fungal molecules and showed that CO4-, CO8- and myc-LCO-induced Ca^{2+} elevations are distinct for their localization, dynamics and plant genetic requirements.

Materials and Methods

Molecular cloning and bacterial transformation

The nucleotide sequence encoding the bioluminescent Ca^{2+} indicator aequorin fused to Yellow Fluorescent Protein (YFP) and targeted to either the cytosol-only (CPK17G2A) or nucleus-only (NLS-YA) (Mehlmer *et al.*, 2012) were amplified with Q5 DNA polymerase (NEB) according to the instruction manual. The promoter (1100 bp upstream of the ATG) of ubiquitin10 was amplified from the genome of *Lotus japonicus* (*Gifu* ecotype). Primers (listed in Table S1) were designed to be compatible with the GreenGate cloning system and cloning of the entry vectors was performed according to it (Lampropoulos *et al.*, 2013). Expression vectors were assembled via cut-ligation with BsaI (NEB) and T4-DNA ligase (NEB), following the GreenGate protocol. The selection and amplification of vectors were performed in DH5α *E. coli* cells. The sequences were checked via Sanger sequencing at BMR Genomics (Padova, Italy) and by Primordium long-read DNA

sequencing at Primordium Labs (Arcadia, CA, USA). The expression vectors were then transformed into *Agrobacterium rhizogenes 1193* via the freeze & thaw method (Wise *et al.*, 2006). Expression vectors are listed in Table S2.

Generation of *Lotus japonicus* transgenic roots

Lotus japonicus ecotype Gifu seeds were scarified with sandpaper and sterilized in 0.5% (w/v) sodium hypochlorite for 11 min. Seeds were then rinsed and washed 5 times in sterile distilled water. For germination, seeds were placed into sterile Petri dishes with H_2O with plant agar 1% (w/v) and wrapped in aluminum foil. After 3 days at 23°C, young seedlings were transferred to square plates (12x12 cm) containing ½ strength B5 growth medium, supplemented with 0.8% (w/v) plant agar and adjusted to pH 5.5 with 1 M KOH. Plates were grown vertically under long-day conditions (23°C, 16 h light/8 h dark cycle). After 3 days, the seedlings were transformed via *Agrobacterium rhizogenes 1193* - mediated hairy root transformation (Boisson-Dernier *et al.*, 2001). The root was cut off with a blade and the wound was dipped into a fully grown plate of *A. rhizogenes* carrying the plasmid of interest. The infected shoots were then placed onto square plates (12x12) containing ½ strength B5 growth medium, 0.8% plant agar, pH 5.5. After 16 h in the darkness, seedlings were co-cultivated with bacteria for 3 days. Afterward, the seedlings were transferred into new squared plates with the same medium supplemented with 300 mg/ml cefotaxime and 0.1% Plant Preservative Mixture (PPM, Duchefa) under long-day conditions (23°C, 16 h light/8 h dark cycle). After 3 weeks, transformed roots were checked for expression of the transformation marker (pAtUBQ10*::*mCherry) using the stereomicroscope MZ16F (Leica). The intracellular localization of the probe was confirmed by confocal microscopy observations (Zeiss LSM900 Airyscan2). Transformed plants were kept in the same growth medium under long-day conditions (23°C, 16 h light/8 h dark cycle).

Aequorin-based Ca^{2+} measurement assays

For Ca^{2+} measurement assays in *L. japonicus* composite plants, 5 mm segments of transformed roots expressing aequorin targeted to either the cytosol or nucleus were reconstituted overnight with 5 mM coelenterazine. On the following day, after extensive washing, each root piece was placed in the dark chamber of a custom-built luminometer (Electron Tubes) containing a 9893/350A photomultiplier (Thorn EMI). The root was placed in 50 µl H_2O and challenged by injection of an equal volume of a 2-fold concentrated solution for each tested stimulus: CO4, CO8 (IsoSep), mycLCOs (equimolar mix of both non-sulfated and sulfated C16:0 and C18:1). The stock solutions were 10^{-3}M in 50% ethanol for CO4, 10^{-4}M in 50% ethanol for CO8, 10^{-3}M in DMSO for

mycLCOs. Controls were performed by injecting an equal volume of the solvents in which the stimuli are dissolved at the working concentration. Ca^{2+} dynamics were recorded for a total of 30 min before the injection of 100 µL of the discharge solution (30%, v/v, ethanol, 1 M $CaCl_2$). The light signal was collected and converted offline into Ca^{2+} concentration values using a computer algorithm based on the Ca^{2+} response curve of aequorin (Brini *et al.*, 1995). All Ca^{2+} concentration values for each biological replicate are available (Table S3). For pharmacological analyses, the root pieces, before challenge with chito-oligomers, were pre-treated with the pharmacological agents for different time intervals: 1.5 mM $LaCl_3$ (Sigma) and 2 mM EGTA (Sigma) for 10 min, 50 µM cyclopiazonic acid (CPA, stock solution 30 mM in DMSO) for 1 h, 10 µM VAC1 (stock solution 10^{-3}M in DMSO) for 2.5 h (Dünser *et al.*, 2021).

Statistical analysis and data visualization

Data were statistically analyzed and presented graphically using R statistical environment and Rstudio. When passing its assumptions, the Anova test and Tukey's posthoc test was applied, in the other cases, Kruskal Wallins and Dunn't tests were performed. Raw data (Table S3) and R scripts (Files S1-S3) ensure full reproducibility of statistical analysis and plots.

Results

Fungal signals activate distinct Ca^{2+} transients in the cytosol and nucleus of *L. japonicus* roots

To monitor intracellular Ca^{2+} dynamics in *L. japonicus* roots, we assembled expression cassettes for YFP-tagged aequorin reporters specifically targeted to either the cytosol or the nucleus (Mehlmer *et al.*, 2012) under the control of the *LjUBI10* promoter (Fig. S1). The constructs were inserted into *L. japonicus* Gifu background via *A. rhizogenes*-mediated hairy roots transformation and the correct localization of the Ca^{2+} probes was confirmed by fluorescence microscopy analyses (Fig. S1). Root segments from the *L. japonicus* composite plants were then challenged with the purified fungal signals CO4 (short-chain COs), CO8 (long-chain COs) and mycLCOs (sulfated and non-sulfated lipo-COs mixture), and the changes in intracellular [Ca^{2+}] were measured. All categories of chitin-based oligomers were found to trigger stimulus-specific cytosolic Ca^{2+} signatures, varying according to the intensity and timing of the Ca^{2+} increase. In particular, CO4 transiently induced the cytosolic Ca^{2+} characterized by the highest magnitude and earliest occurrence of the peak (Fig. 1a,c and File S1). Notably, the overall shape of the observed cytosolic Ca^{2+} dynamics looks biphasic and resembles the one triggered by germinating spore exudates of *Gigaspora margarita* (Navazio *et al.*, 2007; Moscatiello *et al.*, 2018). CO4, mycLCOs, and CO8 were also found to induce Ca^{2+} transients

in the nucleus (Fig. 1b,d), confirming the activation of nuclear Ca^{2+} responses by short-chain COs (Genre *et al.*, 2013; Sun *et al.*, 2015) and long-chain COs (Feng *et al.*, 2019) monitored with Cameleon. Interestingly, no significant differences could be detected in either overall shape or peak intensity among the nuclear-induced Ca^{2+} transients among the three categories of microbial signals (Fig. 1 and File S1). Compared to the cytosolic Ca^{2+} transients, which looked distinguishable among the stimuli, the nuclear Ca^{2+} responses appeared to be slower, characterized by a dome-shaped increase, prolonged over time and almost superimposable among the stimuli, consistently with the results of the statistical test on the Ca^{2+} concentration at the peak (Fig. 1).

Ca^{2+} signatures triggered by chitin-derived oligomers differentially depend on the Common Symbiotic Signalling Pathway

To evaluate the contribution of the CSSP to the different intracellular Ca^{2+} signals triggered in *L. japonicus* roots by the above-mentioned fungal molecules, we conducted Ca^{2+} measurement assays in *L. japonicus symrk* and *castor* mutants, lacking well-established components of the CSSP pathway (Oldroyd, 2013; Choi *et al.*, 2018; Radhakrishnan *et al.*, 2020). The cytosolic Ca^{2+} transients induced by either CO4 or CO8 showed a trend of increased $[Ca^{2+}]$ at the peak in the CSSP mutants compared to the wild-type (Fig. 2a-d and File S2). By contrast, transients induced by mycLCOs completely overlap among the three genotypes (Fig. 2e,f and File S2). On the other hand, major changes were found in the nuclear Ca^{2+} transients triggered by the above-considered microbial molecules among the different genetic backgrounds (Fig. 3a-f and Fig. S2). Indeed, in the *symrk* and *castor* mutants, CO4 and mycLCOs induced only an initial and steep $[Ca^{2+}]_{nuc}$ change but not the subsequent dome-shaped and prolonged Ca^{2+} elevation that was present in the wild-type. This observation led us to further analyse and dissect the evoked Ca^{2+} transients in three different time intervals: total, Phase 1 (0-10 minutes after stimulus) and Phase 2 (10-30 minutes after stimulus). In particular, the sustained $[Ca^{2+}]_{nuc}$ increase observable in the wild-type during Phase 2 mirrors the non-synchronous Ca^{2+}-spiking previously observed by using cameleon-based Ca^{2+} probes (Genre *et al.*, 2013; Feng *et al.*, 2019), as this characteristic Ca^{2+} dynamics is abolished in CSSP mutants. Notably, the nuclear Ca^{2+} transients evoked by CO8 stimulation is only partially affected in the *symrk* and *castor* mutants (Fig. 3c-d).

To further dissect the complexity of the Ca^{2+} traces, we plotted the maximum peak against integral $[Ca^{2+}]$ values in the two phases, both in the cytosol and in the nucleus (Fig. S2). We observed that the Ca^{2+} signals induced by chitin-derived fungal molecules form different clusters according to the considered time phase and intracellular location. Intriguingly, CO4-induced Ca^{2+} responses group

together with those triggered by CO8 in cytosolic Phase 1 and with mycLCOs in nuclear Phase 2, especially in the *symrk* background (Fig. S2).

Origin and modulation of the CO4-induced Ca^{2+} fluxes

As CO4 triggered the most intense and sustained Ca^{2+} response, we used this molecule to elucidate the source and potential interdependence of the observed nuclear and cytosolic Ca^{2+} fluxes with a pharmacological approach. $LaCl_3$ treatment caused a complete abolishment of the Ca^{2+} response to CO4 in both the cytosol (Fig. 4a,c and File S3) and nucleus (Fig. 4b,d and File S3). On the other hand, in the presence of the extracellular Ca^{2+} chelator EGTA, the earliest Ca^{2+} peak, characteristic of the first phase of the Ca^{2+} change, was almost abolished in the cytosol (Fig. 4a,c and File S3) but retained in the nucleus (Fig. 4b,d and File S3).

To misregulate Ca^{2+} homeostasis in the plant endomembrane system, cyclopiazonic acid (CPA) and VAC1 (Dünser *et al.*, 2021) were used to target the endoplasmic reticulum (ER) and the vacuole, respectively. CPA is an inhibitor of ER-type Ca^{2+} ATPases (ECA1) present in the ER membrane, thus causing the ER lumen Ca^{2+} depletion (De Vriese *et al.*, 2018; Cortese *et al.*, 2022). After 1 h pre-treatment with CPA, the first rapid cytosolic Ca^{2+} elevation evoked by CO4 was not only maintained but also actually increased (Fig. 4a,c and File S3). This result suggests that the ER acts as a sink, rather than a source, for the Ca^{2+} fluxes underlying the first cytosolic Ca^{2+} peak. Notably, the nuclear Ca^{2+} transient is completely abolished by pre-treatment with CPA (Fig. 4b,d and File S3); this is consistent with the crucial role played by the nuclear envelope, in continuity with the ER lumen, to generate the Ca^{2+} fluxes giving rise to nuclear and perinuclear Ca^{2+} spiking (Capoen *et al.*, 2011).

VAC1 is an inhibitor of SNARE-dependent vesicle fusions. Thereby, VAC1 treatment reduces cargo and membrane delivery to the vacuole, consequently reducing the size of the vacuole (Dünser *et al.*, 2021). After 2.5 h pre-treatment of *L. japonicus* roots with VAC1, the first Ca^{2+} peak observed upon challenge with CO4 was found to be extremely enhanced (Fig. 4a,c and File S3), suggesting that alterations in vacuolar function may lead to a reduced organellar Ca^{2+} uptake from the cytosol. On the other hand, the nuclear Ca^{2+} transient was largely unaffected in VAC1 pre-treated roots (Fig. 4b,d and File S3), thereby highlighting that the vacuole is not involved in the generation or maintenance of nuclear Ca^{2+}-spiking.

To sum up, our pharmacological analyses further showed that the CO4-induced cytosolic and nuclear Ca^{2+} transients are made of two distinct phases, which are either partially (Phase 1) or completely dependent (Phase 2) on Ca^{2+} influx from the apoplast.

Discussion

Ca^{2+} is a crucial intracellular transducer for the activation of plant responses to microbes. A cytosolic Ca^{2+} influx is pivotal for plant immunity-like responses, but it is also induced by symbiotic microorganisms. On the other hand, nuclear and perinuclear Ca^{2+} spiking events are traditionally considered as marker plant responses to symbiotic signals, although nuclear Ca^{2+} oscillations have recently been detected also in response to pathogenic signals and during developmental processes (Zipfel & Oldroyd, 2017; Leitão *et al.*, 2019).

In this work we identified complex and multiphasic compartment-specific Ca^{2+} signatures activated in response to different fungal signals in *L. japonicus*. Aequorin-based Ca^{2+} measurement assays demonstrated that short-chain (CO4), long-chain (CO8) and lipidated (mycLCOs) chitooligosaccharides are all able to induce both cytosolic and nuclear Ca^{2+} transients (Fig. 1). Analyzing *L. japonicus* mutants of the CSSP, we observed two distinct temporal phases in the Ca^{2+} responses, which exhibited different genetic requirements for the different diffusible fungal signals (Figs. 2,3). Based on our results, the classical separation of fungal molecules into clear-cut symbiotic and pathogenic categories seems reductionist, since the dynamics of the Ca^{2+} signals triggered by chitin-derived molecules look time-, phase-, and compartment-dependent, with a differential clustering of the Ca^{2+} traces elicited by CO4, CO8 and mycLCOs when both [Ca^{2+}] peak and [Ca^{2+}] integral are taken into account (Fig. S2). Indeed, in the prolonged nuclear Phase 2, which represents the well-known nuclear Ca^{2+} spiking, CO4 and mycLCO activated similar Ca^{2+} responses, as expected. In our experimental setup, CO8 activated a very similar response in the wild-type, consistent with recent evidence in *Medicago truncatula* and rice (Feng *et al.*, 2019; Zhang *et al.*, 2021). On the other hand, the CO8-induced Ca^{2+} response was completely independent of SYMRK and only partially dependent on CASTOR, highlighting that in nuclear Phase 2 CO4 and mycLCOs behave differently from CO8.

Despite the recently suggested role as a symbiotic molecule, CO8 has long been considered one of the canonical fungal PAMPs (Cao *et al.*, 2014; Bjornson *et al.*, 2021). With our setup, we indeed found a CO8-elicited cytosolic Ca^{2+} elevation, which showed an increased peak in *symrk* and *castor*. Intriguingly, a similar pattern was found for CO4, but not for mycLCOs. Thereby, in the cytosol CO4 activates a Ca^{2+} response that is closer to CO8 than to mycLCOs. The biological meaning of this compartment-and time- specific differential clustering of Ca^{2+} traces triggered by fungal elicitors needs to be further investigated. However, considering the recently reported interplay between symbiotic and immunity pathways via a SYMRK-BAK1 module (Feng *et al.*, 2021), we may speculate that in the absence of the CSSP there is an increased immunity response,

represented by the much sharper early cytosolic Ca^{2+} response. Moreover, this enhanced Ca^{2+} transient in Phase 1 is associated with a reduced nuclear Ca^{2+} spiking, suggesting the existence of a possible feedback control mechanism between the cytosolic and nuclear Ca^{2+} responses activated by fungal molecules.

The nuclear and perinuclear Ca^{2+} spiking events are known to originate from the Ca^{2+} stored in the nuclear envelope, via the concerted activity of Ca^{2+}-permeable channels and Ca^{2+} pumps (Zipfel & Oldroyd, 2017; Charpentier, 2018). The results obtained by pre-treating *L. japonicus* roots with the IIA ER-type Ca^{2+}-ATPase inhibitor CPA supported the participation of this intracellular Ca^{2+} storage compartment in the observed Ca^{2+} fluxes (Fig. 4), as previously reported in response to Nod factors (Capoen *et al.*, 2011). On the other hand, the first phase of the cytosolic Ca^{2+} transient triggered by CO4 is generated by an influx of the ion from the apoplast, as showed by its inhibition with $LaCl_3$ and EGTA (Fig. 4). These data confirm and extend previous reports in soybean and *L. japonicus* cell suspension cultures (Navazio *et al.*, 2007; Francia *et al.*, 2011). Intriguingly, the nuclear Phase 1 was still found to be activated in the presence of EGTA. This result could be explained by the necessity for Ca^{2+} influx to establish the prolonged nuclear Ca^{2+} response. On the other hand, the Ca^{2+} influx itself is not sufficient to activate it. Thereby, as it has been previously shown for Nod-factor (Shaw & Long, 2003; Morieri *et al.*, 2013), short-chain COs induce a remarkable Ca^{2+} influx that may be involved in the activation of both CSSP and parallel pathways. The precise role of this early Ca^{2+} influx in the establishment of AM symbiosis needs further investigations.

Our data uncovered a cross-talk between the cytosolic and nuclear Ca^{2+} fluxes, highlighting the participation of not only the ER, but also the vacuole, in shaping intracellular Ca^{2+} dynamics. Indeed, the use of VAC1, a newly developed drug affecting membrane delivery to the vacuole and thereby vacuolar size (Dunser et al., 2021), suggested the involvement of the vacuole in the dissipation of the early cytosolic Ca^{2+} rise induced by CO4. The application of the recently designed aequorin-based (Cortese *et al.*, 2022) and GCaMP-based (Luo *et al.*, 2020; Resentini *et al.*, 2021) probes targeted to the plant ER, together with yet-to-develop GECIs for Ca^{2+} measurements/imaging inside the vacuolar lumen, will help uncover the contribution of these mobilizable Ca^{2+} pools to the pathogenic and symbiotic plant Ca^{2+} signalling network.

Acknowledgements

We thank Ute Vothknecht (University of Bonn, Germany) for the CPK17G2A-NES-YA and NLS-YA plasmids, Marco Incarbone and Mattia Donà (Gregor Mendel Institute, Vienna, Austria) for the

destination vector, and Sébastien Fort (CNRS, Paris, France) for the mycLCOs. We are grateful to Lene Heegaard Madsen and Jens Stougaard (Aarhus University, Denmark) for kindly providing *L. japonicus symrk* and *castor* mutants. The technical assistance of the Imaging Facility and the Plant Genome Editing Facility of the Department of Biology (University of Padova, Italy) is gratefully acknowledged. This work was supported by grants from the University of Padova, Italy (PRID prot. BIRD180317 to LN; PRID prot. BIRD214519, PRID Seed Giovani to FB), from the European Union - NextGenerationEU (2021 STARS Grants@Unipd programme P-NICHE to MG) and the Austrian Science Fund (FWF; P 33044 to JK-V), and German Science fund (DFG; 470007283 and CIBSS-EXC-2189 to JK-V).

Author contributions

LN and MG conceived the study and designed research; FB conducted most of the experiments; FB and MG analyzed data and conducted statistical analyses; FB, MG and LN wrote the paper. JKV provided materials and contributed to the discussion and manuscript editing.

ORCID

Filippo Binci https://orcid.org/0000-0002-9030-2496
Jürgen Kleine-Vehn https://orcid.org/0000-0002-4354-3756
Marco Giovannetti https://orcid.org/0000-0001-5305-0341
Lorella Navazio https://orcid.org/0000-0001-5640-108X

Data availability

The data that support the findings of this study are available within the paper and in its Supporting Information.

References

Bjornson M, Pimprikar P, Nürnberger T, Zipfel C. **2021**. The transcriptional landscape of *Arabidopsis thaliana* pattern-triggered immunity. *Nature Plants* **7**: 579–586.

Boisson-Dernier A, Chabaud M, Garcia F, Bécard G, Rosenberg C, Barker DG. **2001**. *Agrobacterium rhizogenes*-transformed roots of *Medicago truncatula* for the study of nitrogen-

fixing and endomycorrhizal symbiotic associations. *Molecular Plant-Microbe Interactions: MPMI* **14**: 695–700.

Brini M, Marsault R, Bastianutto C, Alvarez J, Pozzan T, Rizzuto R. **1995**. Transfected aequorin in the measurement of cytosolic Ca^{2+} concentration ($[Ca^{2+}]_c$): a critical evaluation. J*ournal of Biological Chemistry* **270**: 9896–9903.

Cao Y, Liang Y, Tanaka K, Nguyen CT, Jedrzejczak RP, Joachimiak A, Stacey G. **2014**. The kinase LYK5 is a major chitin receptor in Arabidopsis and forms a chitin-induced complex with related kinase CERK1. *eLife* **3**.

Capoen W, Sun J, Wysham D, Otegui MS, Venkateshwaran M, Hirsch S, Miwa H, Downie JA, Morris RJ, Ané J-M, *et al.* 2011. Nuclear membranes control symbiotic calcium signaling of legumes. *Proceedings of the National Academy of Sciences* **108**: 14348–14353.

Carotenuto G, Chabaud M, Miyata K, Capozzi M, Takeda N, Kaku H, Shibuya N, Nakagawa T, Barker DG, Genre A. **2017**. The rice LysM receptor-like kinase OsCERK1 is required for the perception of short-chain chitin oligomers in arbuscular mycorrhizal signaling. *New Phytologist* **214**: 1440–1446.

Charpentier M. **2018**. Calcium signals in the plant nucleus: origin and function. *Journal of Experimental Botany* **69**: 4165–4173.

Choi J, Summers W, Paszkowski U. **2018**. Mechanisms underlying establishment of arbuscular mycorrhizal symbioses. *Annual Review of Phytopathology* **56**: 135–160.

Cortese E, Moscatiello R, Pettiti F, Carraretto L, Baldan B, Frigerio L, Vothknecht UC, Szabo I, De Stefani D, Brini M, *et al.* 2022. Monitoring calcium handling by the plant endoplasmic reticulum with a low-Ca^{2+}-affinity targeted aequorin reporter. *The Plant Journal* **109**: 1014–1027.

Costa A, Navazio L, Szabo I. **2018**. The contribution of organelles to plant intracellular calcium signalling. *Journal of Experimental Botany*. **17**: 4175-4193.

De Vriese K, Costa A, Beeckman T, Vanneste S. **2018**. Pharmacological strategies for manipulating plant Ca^{2+} signalling. *International Journal of Molecular Sciences* **19**: 1506.

Dünser K, Schöller M, Löfke C, Xiao N, Pařízková B, Melnik S, Stöger E, Novák O, Kleine-Vehn J. **2021**. Endocytic trafficking promotes vacuolar enlargements for fast cell expansion rates in plants. *bioRxiv*. doi: 10.1101/2021.11.29.470358

Feng F, Sun J, Radhakrishnan GV, Lee T, Bozsóki Z, Fort S, Gavrin A, Gysel K, Thygesen MB, Andersen KR, *et al.* 2019. A combination of chitooligosaccharide and lipochitooligosaccharide recognition promotes arbuscular mycorrhizal associations in *Medicago truncatula*. *Nature Communications* **10**: 5047.

Feng Y, Wu P, Liu C, Peng L, Wang T, Wang C, Tan Q, Li B, Ou Y, Zhu H, *et al.* 2021. Suppression of LjBAK1-mediated immunity by SymRK promotes rhizobial infection in *Lotus japonicus*. *Molecular Plant* **14**: 1935–1950.

Francia D, Chiltz A, Lo Schiavo F, Pugin A, Bonfante P, Cardinale F. **2011**. AM fungal exudates activate MAP kinases in plant cells in dependence from cytosolic Ca^{2+} increase. *Plant Physiology and Biochemistry* **49**: 963–969.

Genre A, Chabaud M, Balzergue C, Puech-Pagès V, Novero M, Rey T, Fournier J, Rochange S, Bécard G, Bonfante P, *et al.* 2013. Short-chain chitin oligomers from arbuscular mycorrhizal fungi trigger nuclear Ca^{2+} spiking in *Medicago truncatula* roots and their production is enhanced by strigolactone. *New Phytologist* **198**: 190–202.

Keinath NF, Waadt R, Brugman R, Schroeder JI, Grossmann G, Schumacher K, Krebs M. **2015**. Live cell Imaging with R-GECO1 sheds light on flg22- and chitin-induced transient $[Ca^{2+}]_{cyt}$ patterns in Arabidopsis. *Molecular Plant* **8**: 1188–1200.

Lampropoulos A, Sutikovic Z, Wenzl C, Maegele I, Lohmann JU, Forner J. **2013**. GreenGate - a novel, versatile, and efficient cloning system for plant transgenesis. *PLoS One* **8**: e83043.

Leitão N, Dangeville P, Carter R, Charpentier M. **2019**. Nuclear calcium signatures are associated with root development. *Nature Communications* **10**: 4865.

Luo J, Chen L, Huang F, Gao P, Zhao H, Wang Y, Han S. **2020**. Intraorganellar calcium imaging in Arabidopsis seedling roots using the GCaMP variants GCaMP6m and R-CEPIA1er. *Journal of Plant Physiology* **246–247**: 153127.

Maillet F, Poinsot V, André O, Puech-Pagès V, Haouy A, Gueunier M, Cromer L, Giraudet D, Formey D, Niebel A, *et al.* 2011. Fungal lipochitooligosaccharide symbiotic signals in arbuscular mycorrhiza. *Nature* **469**: 58–63.

Mehlmer N, Parvin N, Hurst CH, Knight MR, Teige M, Vothknecht UC. **2012**. A toolset of aequorin expression vectors for in planta studies of subcellular calcium concentrations in *Arabidopsis thaliana*. *Journal of Experimental Botany* **63**: 1751–1761.

Miwa H, Sun J, Oldroyd GED, Downie JA. **2006**. Analysis of Nod-factor-induced calcium signaling in root hairs of symbiotically defective mutants of *Lotus japonicus*. *Molecular Plant-Microbe Interactions* **19**: 914–923.

Miyata K, Kozaki T, Kouzai Y, Ozawa K, Ishii K, Asamizu E, Okabe Y, Umehara Y, Miyamoto A, Kobae Y, *et al.* 2014. The bifunctional plant receptor, OsCERK1, regulates both chitin-triggered immunity and arbuscular mycorrhizal symbiosis in rice. *Plant & Cell Physiology* **55**: 1864–1872.

Morieri G, Martinez EA, Jarynowski A, Driguez H, Morris R, Oldroyd GED, Downie JA. **2013**. Host-specific Nod-factors associated with *Medicago truncatula* nodule infection differentially induce calcium influx and calcium spiking in root hairs. *New Phytologist* **200**: 656–662.

Moscatiello R, Sello S, Ruocco M, Barbulova A, Cortese E, Nigris S, Baldan B, Chiurazzi M, Mariani P, Lorito M, *et al.* 2018. The hydrophobin HYTLO1 secreted by the biocontrol fungus *Trichoderma longibrachiatum* triggers a NAADP-mediated calcium signalling pathway in *Lotus japonicus*. *International Journal of Molecular Sciences* **19**: 2596.

Nars A, Lafitte C, Chabaud M, Drouillard S, Mélida H, Danoun S, Costaouëc TL, Rey T, Benedetti J, Bulone V, *et al.* 2013. Aphanomyces euteiches cell wall fractions containing novel glucan-chitosaccharides induce defense genes and nuclear calcium oscillations in the plant host *Medicago truncatula*. *PLoS One* **8**: e75039.

Navazio L, Moscatiello R, Genre A, Novero M, Baldan B, Bonfante P, Mariani P. **2007**. A diffusible signal from arbuscular mycorrhizal fungi elicits a transient cytosolic calcium elevation in host plant cells. *Plant Physiology* **144**: 673–681.

Oldroyd GED. **2013**. Speak, friend, and enter: signalling systems that promote beneficial symbiotic associations in plants. *Nature Reviews Microbiology* **11**: 252–263.

Pirayesh N, Giridhar M, Ben Khedher A, Vothknecht UC, Chigri F. **2021**. Organellar calcium signaling in plants: An update. *Biochimica et Biophysica Acta - Molecular Cell Research* **1868**: 118948.

Radhakrishnan GV, Keller J, Rich MK, Vernié T, Mbadinga Mbadinga DL, Vigneron N, Cottret L, Clemente HS, Libourel C, Cheema J, *et al.* 2020. An ancestral signalling pathway is conserved in intracellular symbioses-forming plant lineages. *Nature Plants* **6**: 280–289.

Ranf S, Eschen-Lippold L, Pecher P, Lee J, Scheel D. **2011**. Interplay between calcium signalling and early signalling elements during defence responses to microbe- or damage-associated molecular patterns. *The Plant Journal* **68**: 100–113.

Resentini F, Grenzi M, Ancora D, Cademartori M, Luoni L, Franco M, Bassi A, Bonza MC, Costa A. **2021**. Simultaneous imaging of ER and cytosolic Ca^{2+} dynamics reveals long-distance ER Ca^{2+} waves in plants. *Plant Physiology* **187**: 603–617.

Shaw SL, Long SR. **2003**. Nod Factor elicits two separable calcium responses in *Medicago truncatula* root hair cells. *Plant Physiology* **131**: 976–984.

Stael S, Wurzinger B, Mair A, Mehlmer N, Vothknecht UC, Teige M. **2012**. Plant organellar calcium signalling: an emerging field. *Journal of Experimental Botany* **63**: 1525–1542.

Sun J, Miller JB, Granqvist E, Wiley-Kalil A, Gobbato E, Maillet F, Cottaz S, Samain E, Venkateshwaran M, Fort S, *et al.* 2015. Activation of symbiosis signaling by arbuscular mycorrhizal fungi in legumes and rice. *The Plant Cell* **27**: 823–838.

Thor K, Peiter E. **2014**. Cytosolic calcium signals elicited by the pathogen-associated molecular pattern flg22 in stomatal guard cells are of an oscillatory nature. *New Phytologist* **204**: 873–881.

Wan J, Tanaka K, Zhang X-C, Son GH, Brechenmacher L, Nguyen THN, Stacey G. **2012**. LYK4, a lysin motif receptor-like kinase, is important for chitin signaling and plant innate immunity in Arabidopsis. *Plant Physiology* **160**: 396–406.

Wise AA, Liu Z, Binns AN. **2006**. Three methods for the introduction of foreign DNA into Agrobacterium. In: Wang K, ed. Methods in Molecular Biology. Agrobacterium Protocols. Totowa, NJ: Humana Press, 43–54.

Zhang X, Dong W, Sun J, Feng F, Deng Y, He Z, Oldroyd GED, Wang E. **2015**. The receptor kinase CERK1 has dual functions in symbiosis and immunity signalling. *The Plant Journal* **81**: 258–267.

Zhang C, He J, Dai H, Wang G, Zhang X, Wang C, Shi J, Chen X, Wang D, Wang E. **2021**. Discriminating symbiosis and immunity signals by receptor competition in rice. *Proceedings of the National Academy of Sciences* **118**: e2023738118.

Zipfel C, Oldroyd GED. **2017**. Plant signalling in symbiosis and immunity. *Nature* **543**: 328–336.

Legends to Figures

Fig. 1 Monitoring of cytosolic and nuclear free [Ca^{2+}] in 5 mm-long root segments from composite plants of *L. japonicus* in response to different chitin-based oligomers.

L. japonicus roots were transformed via *A. rhizogenes* with constructs encoding aequorin chimeras targeted to either the cytosol (a-c) or nucleus (b-d) and subcellular Ca^{2+} dynamics were measured after challenge with 10^{-7}M CO4 (dark blue), 10^{-6}M CO8 (green), 10^{-7} M mycLCOs (light blue). In a-b, data are presented as means ± SE (shading) of n≥6 traces from at least 3 different composite plants (independent transformations). Arrow indicates the time of stimulus injection (time 0). In c-d, dots represent the maximum [Ca^{2+}] value for each trace in the time range of 1-20 minutes. The frequency distributions of the dots are represented on top of the panel (time) and at the right of the panel ([Ca^{2+}]).

Fig. 2 Monitoring of free cytosolic [Ca^{2+}] in 5 mm-long root segments from composite plants of *L. japonicus* in Gifu wt (grey), *castor* (light orange), *symrk* (dark orange).

Ca^{2+} measurements were conducted in response to 10^{-7} M CO4 (a,b), 10^{-6}M CO8 (c,d), 10^{-7}M mycLCOs (e,f). In a,c,e, data are presented as means ± SE (shading) of n≥6 traces from at least 3 different composite plants (independent transformation). Arrows indicate the time of stimulus injection (time 0). In b,d,f, dots represent the maximum [Ca^{2+}]. The black line represents the median of each group.

Fig. 3 Monitoring of free nuclear cytosolic [Ca^{2+}] in 5 mm-long root segments from composite plants of *L. japonicus* in Gifu wt (grey), *castor* (light orange), *symrk* (dark orange).
Ca^{2+} measurements were conducted in the nucleus in response to 10^{-7} M CO4 (a,b), 10^{-6}M CO8 (c,d), 10^{-7}M mycLCOs (e,f). In a,c,e, data are presented as means ± SE (shading) of n≥6 traces from at least 3 different composite plants (independent transformation). Arrows indicate the time of stimulus injection (time 0). The dashed line separates phase 1 (0-10 minutes after stimulus) and phase 2 (10-30 minutes after stimulus). In b,d,f, dots represent the integrated [Ca^{2+}] for each trace in the whole run and in the two different phases. The black line represents the median of each group. Different letters indicate statistically significant differences among groups.

Fig. 4. Pharmacological analyses of short-chain COs-induced Ca^{2+} fluxes in *L. japonicus* roots.
Cytosolic [Ca^{2+}] (a,c) and nuclear [Ca^{2+}] (b,d) dynamics were monitored in 5-mm long root segments from composite plants challenged with 10^{-7} M CO4 after pre-treatment with either 1.5 mM $LaCl_3$ (dark violet), 2 mM EGTA (light violet), 50 μM CPA (dark green), 10 μM VAC1 (light green) or none (grey, either H_2O or solvent control). In a-b, data are presented as means ± SE (shading) of n≥6 traces obtained from at least 3 different composite plants (independent transformation). In c-d, small dots represent the delta maximum cytosolic [Ca^{2+}] ($\Delta[Ca^{2+}]_{cyt}$) (c) and the delta integrated [Ca^{2+}] ($\Delta[Ca^{2+}]_{nuc}$) (d) for each trace in the time range of 2-20 minutes, while the big circles represent the mean. $\Delta[Ca^{2+}]$ was calculated by subtracting the mean of the resting [Ca^{2+}] in the pre-stimulus phase to each [Ca^{2+}] measurement value following the stimulus injection (arrow). The coloured vertical line shows the difference between the mean of each treatment and the control (horizontal grey line).

Supporting Information

Fig. S1 Genetic map and intracellular localization of cytosolic and nuclear YFP-aequorin chimeras.
Fig. S2 Plot of the cytosolic and nuclear maximum peak against integral [Ca^{2+}] values in the Phase 1 and 2.

Table S1 List of primers used in this study.

Table S2 List of plasmids used in this study.

Table S3 Raw data of calcium concentrations.

File S1 R script used for creating figure 1 and its statistical analysis.

File S2 R script used for creating figure 2 and figure 3 and their statistical analysis.

File S3 R script used for creating figure 4 and its statistical analysis.

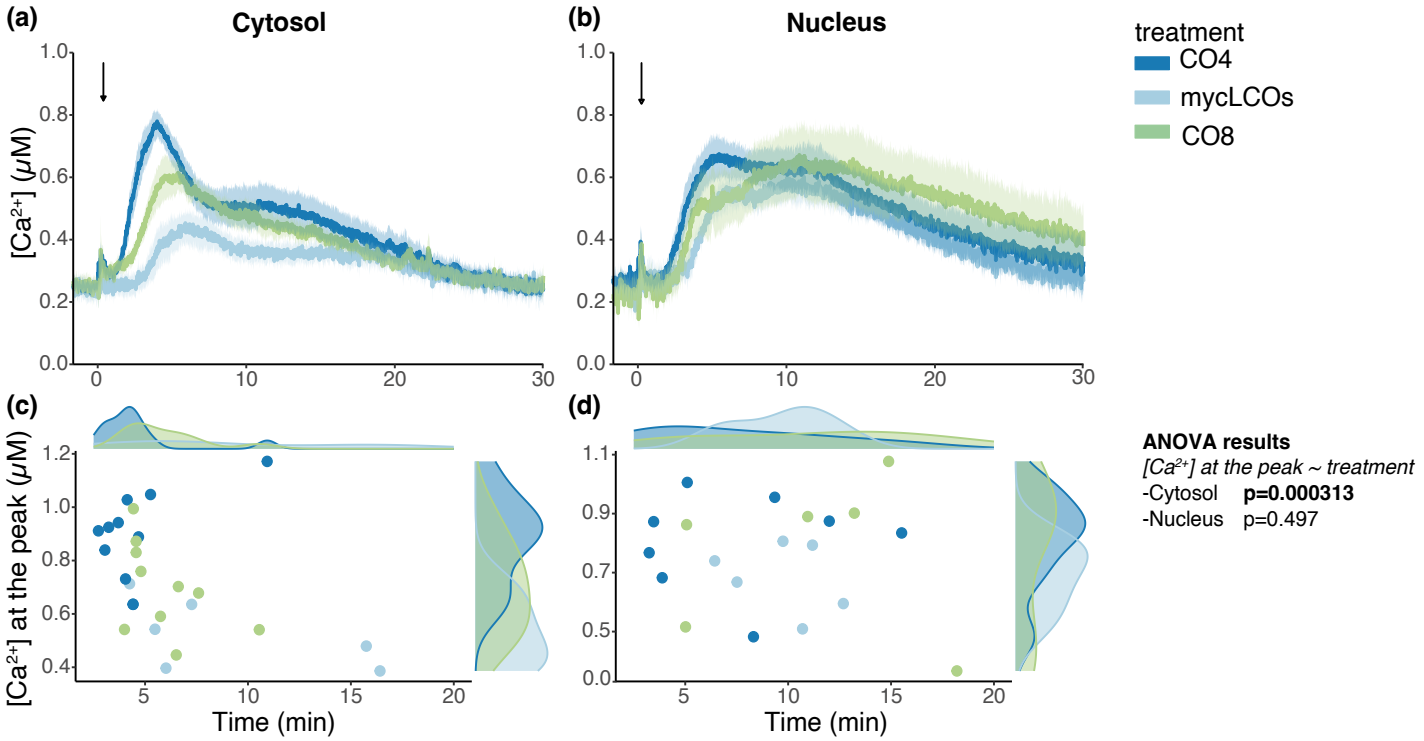

Fig. 1 Monitoring of cytosolic and nuclear free [Ca^{2+}] in 5 mm-long root segments from composite plants of *L. japonicus* in response to different chitin-based oligomers.

L. japonicus roots were transformed via *A. rhizogenes* with constructs encoding aequorin chimeras targeted to either the cytosol (a-c) or nucleus (b-d) and subcellular Ca^{2+} dynamics were measured after challenge with 10^{-7}M CO4 (dark blue), 10^{-6}M CO8 (green), 10^{-7} M mycLCOs (light blue). In a-b, data are presented as means ± SE (shading) of n≥6 traces from at least 3 different composite plants (independent transformations). Arrow indicates the time of stimulus injection (time 0). In c-d, dots represent the maximum [Ca^{2+}] value for each trace in the time range of 1-20 minutes. The frequency distributions of the dots are represented on top of the panel (time) and at the right of the panel ([Ca^{2+}]).

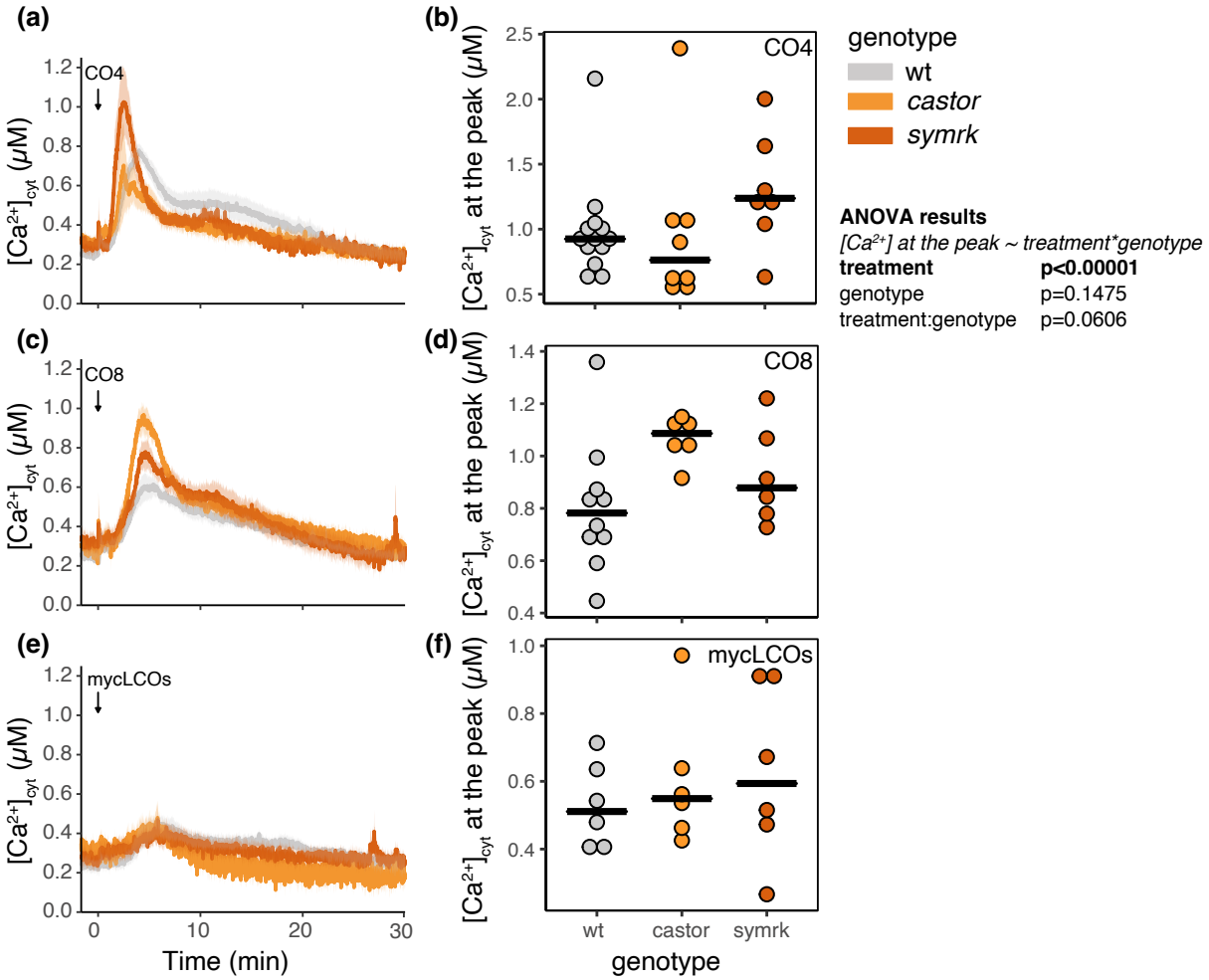

Fig. 2 Monitoring of free cytosolic [Ca^{2+}] in 5 mm-long root segments from composite plants of *L. japonicus* in Gifu wt (grey), *castor* (light orange), *symrk* (dark orange).

Ca^{2+} measurements were conducted in response to 10^{-7} M CO4 (a,b), 10^{-6}M CO8 (c,d), 10^{-7}M mycLCOs (e,f). In a,c,e, data are presented as means ± SE (shading) of n≥6 traces from at least 3 different composite plants (independent transformation). Arrows indicate the time of stimulus injection (time 0). In b,d,f, dots represent the maximum [Ca^{2+}]. The black line represents the median of each group.

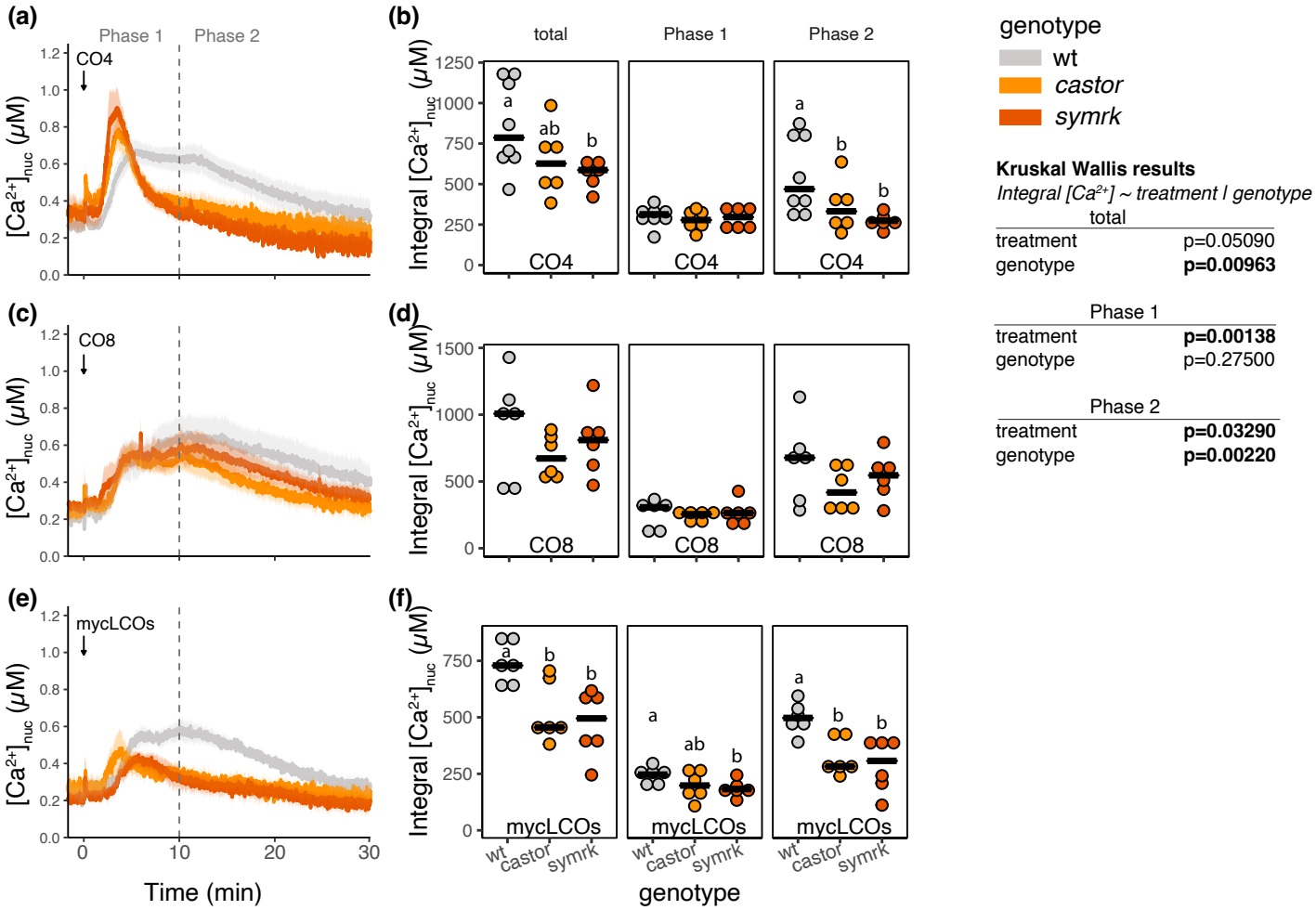

Fig. 3 Monitoring of free nuclear cytosolic [Ca^{2+}] in 5 mm-long root segments from composite plants of *L. japonicus* in Gifu wt (grey), *castor* (light orange), *symrk* (dark orange).

Ca^{2+} measurements were conducted in the nucleus in response to 10^{-7} M CO4 (a,b), 10^{-6}M CO8 (c,d), 10^{-7}M mycLCOs (e,f). In a,c,e, data are presented as means ± SE (shading) of n≥6 traces from at least 3 different composite plants (independent transformation). Arrows indicate the time of stimulus injection (time 0). The dashed line separates phase 1 (0-10 minutes after stimulus) and phase 2 (10-30 minutes after stimulus). In b,d,f, dots represent the integrated [Ca^{2+}] for each trace in the whole run and in the two different phases. The black line represents the median of each group. Different letters indicate statistically significant differences among groups.

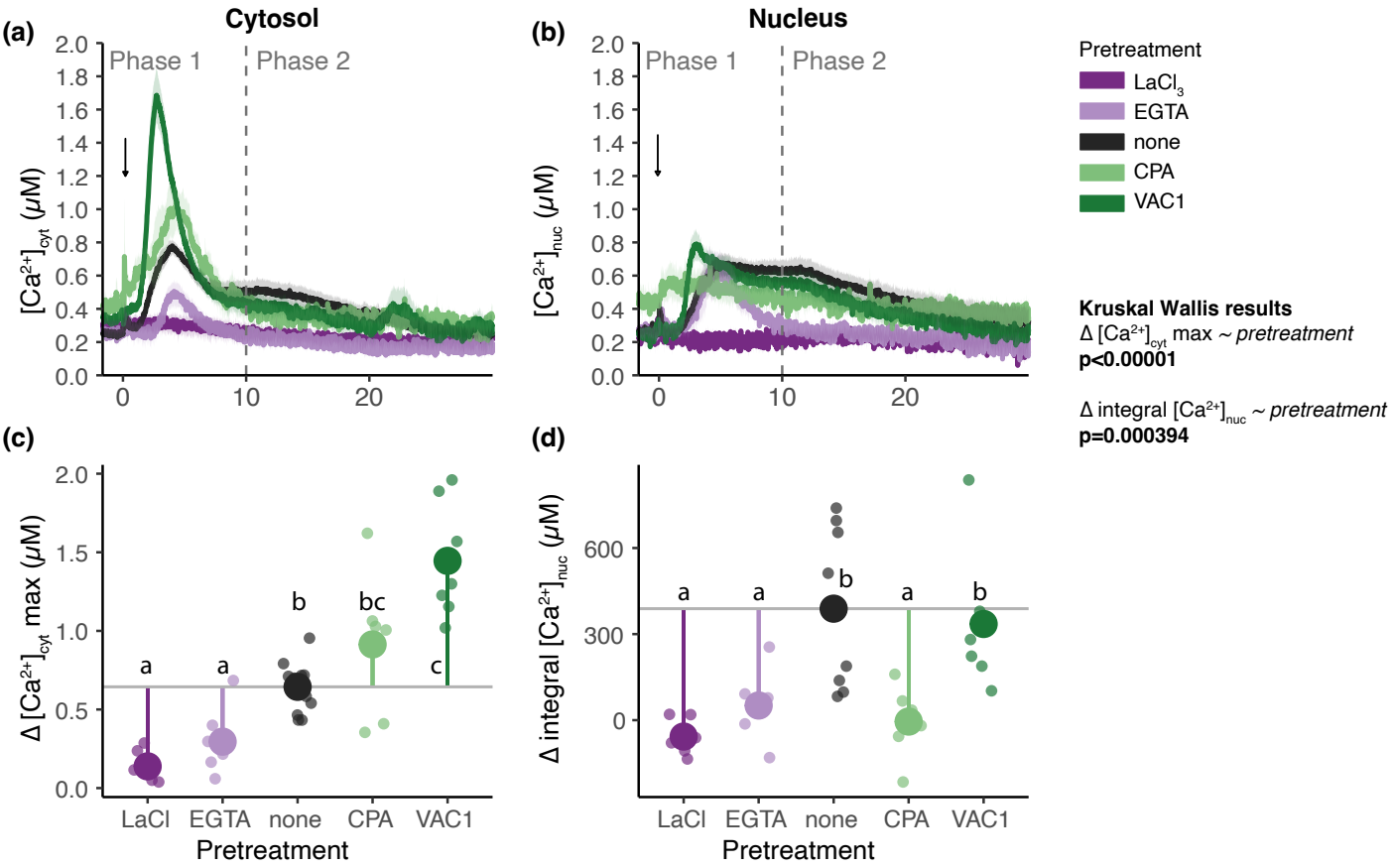

Fig. 4. Pharmacological analyses of short-chain COs-induced Ca^{2+} fluxes in *L. japonicus* roots. Cytosolic [Ca^{2+}] (a,c) and nuclear [Ca^{2+}] (b,d) dynamics were monitored in 5-mm long root segments from composite plants challenged with 10^{-7} M CO4 after pre-treatment with either 1.5 mM $LaCl_3$ (dark violet), 2 mM EGTA (light violet), 50 µM CPA (dark green), 10 µM VAC1 (light green) or none (grey, either H_2O or solvent control). In a-b, data are presented as means ± SE (shading) of n≥6 traces obtained from at least 3 different composite plants (independent transformation). In c-d, small dots represent the delta maximum cytosolic [Ca^{2+}] ($\Delta[Ca^{2+}]_{cyt}$) (c) and the delta integrated [Ca^{2+}] ($\Delta[Ca^{2+}]_{nuc}$) (d) for each trace in the time range of 2-20 minutes, while the big circles represent the mean. $\Delta[Ca^{2+}]$ was calculated by subtracting the mean of the resting [Ca^{2+}] in the pre-stimulus phase to each [Ca^{2+}] measurement value following the stimulus injection (arrow). The coloured vertical line shows the difference between the mean of each treatment and the control (horizontal grey line).